Fermilab FERMILAB-FN-0742 January 2004

FN-0742

ANALYSIS OF FAST STACKING BY RF MANEUVERING

K.Y. Ng

Fermi National Accelerator Laboratory, P.O. Box 500, Batavia, IL 60510*

(December, 2003)

Abstract

Bunch compression by rf maneuvering is analyzed mathematically. The method, proposed by Foster, et al. [1], consists of a rotation by a voltage gradient followed by a shear after reversing the polarity. Barrier pulses are placed at the two ends of the beam all the time to limit undesirable expansion during compression. Simple analytical expressions are derived for several variations of the method.

*Operated by the Universities Research Association, Inc., under contract with the U.S. Department of Energy.

1 INTRODUCTION

To increase the luminosity of the Tevatron at Run II, an important ingredient is to increase the amount of antiprotons produced. [2] To accomplish this, the intensity of the protons in the antiproton-production cycle must be increased. At this moment, the number of protons in one-booster batch is around $84 \times 6 \times 10^{10} = 5.04 \times 10^{12}$. One method under study is slip-stacking,[3] which is designed to double the proton intensity. However, because of severe beam loading, the present goal is to reach an intensity of 8×10^{12}. Up to now, the doubling of 2.5×10^{12} to 5×10^{12} has been achieved. [4] Another method of doubling the proton intensity is to use a moving barrier rf wave [5] and to inject below the nominal energy E_0 by an amount equal to half the energy spread plus

$$\Delta E = \frac{\beta^2 E_0 T_b}{2|\eta| T_{\text{booster}}} = 11.82 \text{ MeV} , \tag{1.1}$$

where $T_b = 1.59$ μs is the booster batch length, $T_{\text{booster}} = 1/15$ s is the booster cycle time, $\eta = -0.008915$ is the Main Injector slip factor at injection computed based on the transition gamma of 21.96. However, this method has not been tested yet.

Foster et al. [1] proposed a simple method of fast stacking by manipulating the rf to compress the beam of total length of two booster batch to one half the size. This essentially stacks two booster batches onto one, thus increasing the intensity of the proton beam for antiproton production. They first employ the three longitudinal dampers [6] in the Main Injector to produce a voltage gradient to rotate the 53-MHz bunches by less than 45° in the normalized longitudinal phase space. The polarity of the voltage gradient is then reversed. The stable fixed point at the center becomes an unstable fixed point. Particles then shear to achieve the required beam compression. Barrier pulses, provided by a Finemat cavity, [7] will be placed on both ends of the beam to limit undesirable expansion of the beam distribution. Experiments had been performed at the Fermilab Recycler Ring to demonstrate the feasibility of the method. [8] This method has long been proposed and simulated in the design of a recirculating induction accelerator for heavy-ion fusion. [9] There, a ramp plus barrier pulses (also known as ear pulses) are employed to compress the time spread of the ion pulses before they hit the target.

In this note, we investigate several variations of this method analytically and present simple analytic formulas for the compression. In Sec. 2, we study beam compression by pure rotation. In Sec. 3, the method involving rotation followed by a shear is analyzed. In Sec. 4,

two barriers pulses are added as suggested by Foster et al. to limit the edge effects of the beam. Conclusion is given in Sec. 5. We end this section by listing in Table I some relevant parameters of the Main Injection at injection.

Table I: Some parameters of the Main Injector at injection.

Circumference (m)	3319.419
Injection energy (GeV)	8.938272
Relativistic γ	9.526309
Relativistic β	0.994471
Revolution frequency f_0 (kHz)	89.81577
Revolution period T_0 (μs)	11.13390
Slip factor η	-0.008915
Booster batch length T_b (μs)	1.590557
Booster repetition rate (Hz)	1/15

2 PURE ROTATION

Theoretically, bunch compression to one-half of its length can be accomplished by a pure rotation in the longitudinal phase space. The advantages are that the procedure is simple and the total longitudinal emittance is preserved. The disadvantage is that the time required can be very long if the initial energy spread is small. The equations of motion are

$$\frac{d\tau}{dt} = \eta\delta \ , \tag{2.1}$$

$$\frac{d\delta}{dt} = \frac{eV_1}{\beta^2 E_0 T_0}\frac{\tau}{T_b} \ , \tag{2.2}$$

where τ is the particle's arrival time ahead of some reference, $T_0 = 7T_b$ is the revolution period of the Main Injector, V_1/T_b is the voltage gradient, which can be supplied by broadband cavities. In the absence of broadband rf cavities, like those in the Recycler Ring, a voltage gradient can be supplied by the longitudinal dampers.† The three longitudinal dampers in

†We refer to the peak voltage supplied by broadband cavities or dampers as V_1 for rotation and $-V_2$ for shear, and the corresponding voltage gradients as V_1/T_b and $-V_2/T_b$, although the two-booster-batch beam may extend over $\pm T_b$ during rotation and shear so that the actual voltages required may exceed V_1 and V_2.

the Main Injector are broadband and can supply up to 1.8 kV. The compression is supposed to be from $2T_b$ to T_b. These equations of motion can be derived from the Hamiltonian

$$H = \frac{\eta}{2}\,\delta^2 - \frac{eV_1}{2\beta^2 E_0 T_0 T_b}\,\tau^2 \ . \tag{2.3}$$

The angular synchrotron frequency is

$$\omega_{s1} = \sqrt{\frac{|\eta| e V_1}{\beta^2 E_0 T_0 T_b}} \ . \tag{2.4}$$

The trajectories can be made into circles if the normalized coordinates $(\tau, -|\eta|\delta/\omega_{s1})$ are chosen. The solution of the Hamiltonian becomes

$$\begin{pmatrix} \tau \\ -\dfrac{|\eta|\delta}{\omega_{s1}} \end{pmatrix}_t = \begin{pmatrix} \cos\omega_{s1}t & \sin\omega_{s1}t \\ -\sin\omega_{s1}t & \cos\omega_{s1}t \end{pmatrix} \begin{pmatrix} \tau \\ -\dfrac{|\eta|\delta}{\omega_{s1}} \end{pmatrix}_0 \tag{2.5}$$

The original beam has half length T_b and half momentum spread δ_0. After a rotation of 90°, the beam is compressed to the new half width of T_b. We therefore have

$$\frac{T_b}{2} = \frac{|\eta|\delta_0}{\omega_{s1}} \ , \tag{2.6}$$

which fixes the synchrotron frequency. The time of rotation then becomes

$$t_1 = \frac{\pi}{2\omega_{s1}} = \frac{\pi T_b}{4|\eta|\delta_0} \ . \tag{2.7}$$

If the initial half-energy spread is $\Delta E = 10$ MeV ($\delta_0 = 0.001131$), this gives $\omega_{s1} = 12.68$ Hz, requiring a peak cavity voltage[‡] of $V_1 = 2.823$ kV. The final momentum spread will be doubled. The rotation time is $t_1 = 0.1239$, which amounts to 1.858 booster cycles, and is rather reasonable. The simulation is shown in Fig. 1.

This rotation time will become longer if the energy spread of the beam starts out to be smaller, as depicted in Fig. 2. For example, at the initial half-energy spread of $\Delta E = 5$ MeV ($\delta_1 = 0.0005656$), the rotation time will be doubled to 3.716 booster cycles, which is too long. One way to reduce the rotation time is to keep the peak rotation voltage always at $V_1 = 2.823$ kV independent of the initial energy spread. Then the rotation time will always be 1.858 booster cycles and the final half-energy spread will always be $\Delta E = 20$ MeV

[‡]Here, peak cavity voltage is just a generic terminology. It can also mean peak damper voltage, depending on the hardware that generates the required voltage gradient.

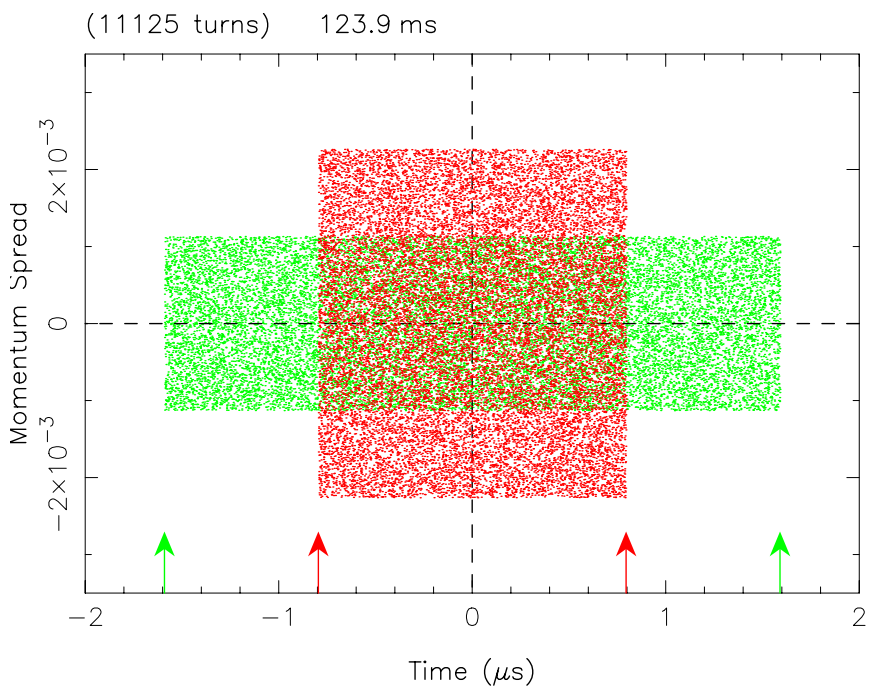

Figure 1: (color) A beam of initial half length T_b and half-energy spread $\Delta E = 10$ MeV ($\delta_0 = 0.001131$), shown in green between the two green arrows, is compressed by one half, shown in red between the two red arrows, via pure 90° rotation. The cavity voltage required is $V_1 = 2.823$ kV and the rotation time is 0.1239 s or 1.858 booster cycles.

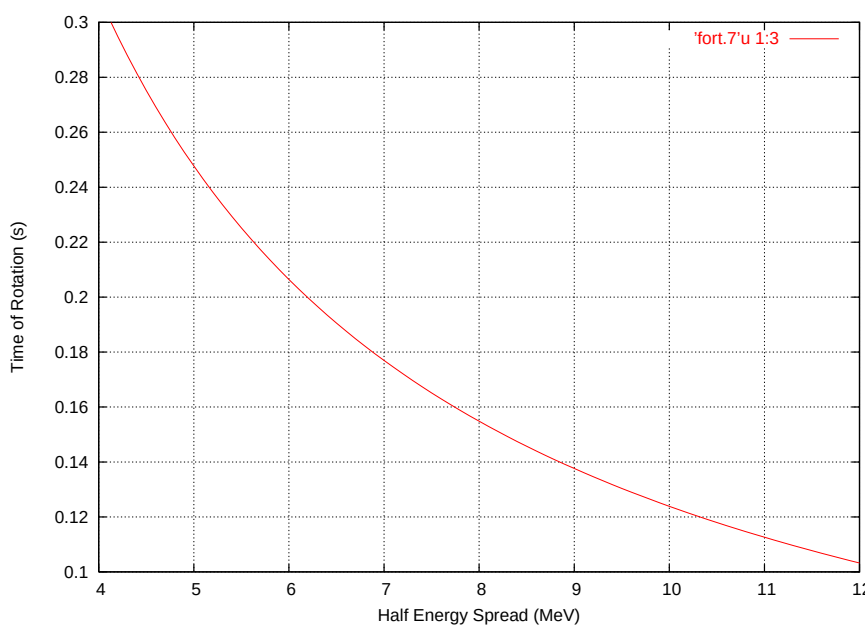

Figure 2: Plot showing the time required for compression as a function of initial half-energy spread of the beam, if a pure rotation is performed.

($\delta = 0.002262$). The only price we need to pay is that the compression will be more than one half. In the case when the initial half-energy spread is $\Delta E = 5$ MeV, the beam composing of two booster batches will be compressed to a total length of $\frac{1}{2}T_b$, half a booster-batch long. The momentum aperture of the Main Injection is about 1% and is large enough to accommodate that. When the compressed beam is recaptured into 53-MHz buckets, however, there will only be 84/2=42 bunches, each of which is 4 times larger in intensity. Thus the effect of beam loading may pose a problem and should be properly addressed.

3 ROTATION FOLLOWED BY A SHEAR

First the beam of half length T_b and half momentum spread δ_0 is rotated at the voltage gradient V_1/T_b for time duration Δt_1. Under this situation, the center of phase space is a stable fixed point and the particles follow elliptical trajectories. The cavity voltage is then switched to $-V_2$ and the beam is allowed to shear for time duration Δt_2 until the half length of the beam is reduced to $T_b/2$. Under this situation, the center of phase space is an unstable fixed point and the beam shears following hyperbolic trajectories. An example with initial half-energy spread $\Delta E = 10$ MeV is illustrated in Fig. 3.

For the initial beam, let us concentrate on the particles having the lowest energy, i.e., those lying along the line AB in Fig. 3. Their positions in the longitudinal phase space are denoted by $(\tau_0, -\delta_0)$ with $|\tau_0| \leq T_b$. After Δt_1, they are rotated under the voltage gradient V_1/T_b into positions denoted by (τ_1, δ_1) according to

$$\begin{pmatrix} \tau_1 \\ -\dfrac{|\eta|\delta_1}{\omega_{s1}} \end{pmatrix} = \begin{pmatrix} \cos\phi_1 & \sin\phi_1 \\ -\sin\phi_1 & \cos\phi_1 \end{pmatrix} \begin{pmatrix} \tau_0 \\ \dfrac{|\eta|\delta_0}{\omega_{s1}} \end{pmatrix} , \tag{3.1}$$

where $\phi_1 = \omega_{s1}\Delta t_1$ is the angle of rotation and the angular synchrotron frequency is given by Eq. (2.4).

Now the cavity voltage is switched to $-V_2$. Although the center of phase space becomes unstable, we can still define the angular synchrotron frequency

$$\omega_{s2} = \sqrt{\frac{|\eta| e V_2}{\beta^2 E_0 T_0 T_b}} . \tag{3.2}$$

The equations of motion become

$$\frac{d\tau}{dt} = -|\eta|\delta , \tag{3.3}$$

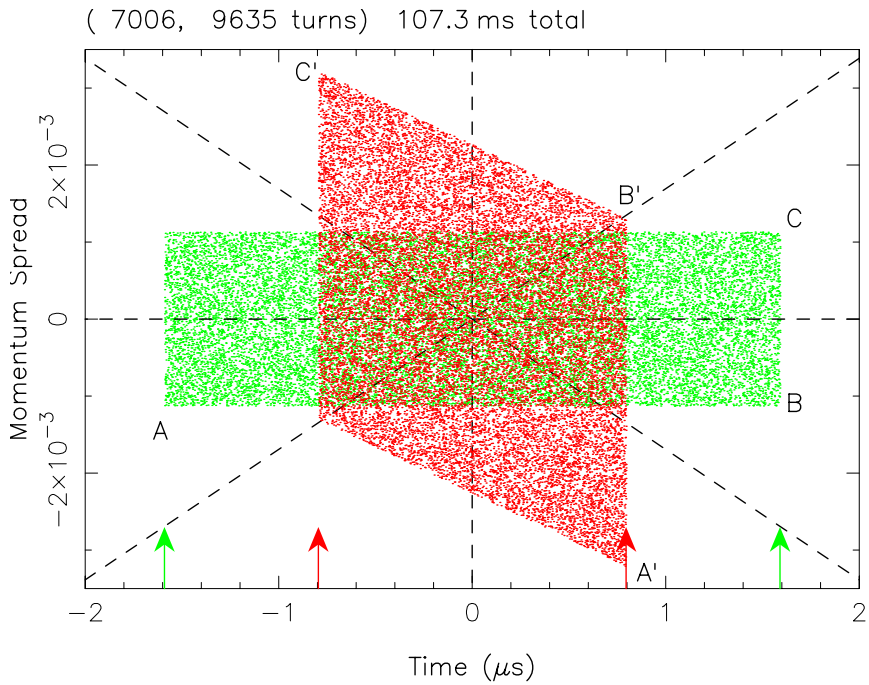

Figure 3: (color) A beam of initial half length T_b and half-energy spread $\Delta E = 10$ MeV ($\delta_0 = 0.001131$), shown in green between the two green arrows, is compressed to one half of its original length, shown in red between the two red arrows, by rotation along elliptical trajectories followed by shear along hyperbolic trajectories. A cavity voltage $V_1 = 4.0$ kV is required for 7006 turns (1.17 booster cycles) in the rotation, while $-V_2 = -4.0$ kV is required for 2628 turns (0.439 booster cycles) in the shear. The slanting dashed lines are the separatrices during the shear.

$$\frac{d\delta}{dt} = -\frac{eV_2}{\beta^2 E_0 T_0}\frac{\tau}{T_b} \ , \tag{3.4}$$

and the particles travel along hyperbolic trajectories. In terms of the normalized coordinates $(\tau, |\eta|\delta/\omega_{s2})$, the solution can be written as

$$\begin{pmatrix} \tau \\ -\dfrac{|\eta|\delta}{\omega_{s2}} \end{pmatrix}_t = \begin{pmatrix} \cosh\omega_{s2}t & \sinh\omega_{s2}t \\ \sinh\omega_{s2}t & \cosh\omega_{s2}t \end{pmatrix} \begin{pmatrix} \tau \\ -\dfrac{|\eta|\delta}{\omega_{s2}} \end{pmatrix}_0 \ . \tag{3.5}$$

The shear motion of the beam takes place in the time interval Δt_2 and particles move from (τ_1, δ_1) to (τ_2, δ_2). We would like all those particles lying along the line AB in Fig. 3 to map onto the line $A'B'$ or to land at $\tau_2 = T_b/2$. We thus obtain

$$\frac{T_b}{2} = \tau_1 \cosh\phi_2 - \frac{|\eta|\delta_1}{\omega_{s2}} \sinh\phi_2 \ , \tag{3.6}$$

where $\phi_2 = \omega_{s2}\Delta t_2$ is the *rotation angle* along the hyperbolic trajectories. Substituting for

(τ_1, δ_1) from Eq. (3.1), the expression becomes

$$\frac{T_b}{2} = \tau_0 \left(\cos\phi_1 \cosh\phi_2 - \frac{\omega_{s1}}{\omega_{s2}} \sin\phi_1 \sinh\phi_2 \right) + \frac{|\eta|\delta_0}{\omega_{s1}} \left(\sin\phi_1 \cosh\phi_2 + \frac{\omega_{s1}}{\omega_{s2}} \cos\phi_1 \sinh\phi_2 \right) . \tag{3.7}$$

Since we expect all particles initially with the lowest energy to arrive at the arrival time $T_b/2$, Eq. (3.7) should be independent of τ_0. We therefore require

$$\cos\phi_1 \cosh\phi_2 = \frac{\omega_{s1}}{\omega_{s2}} \sin\phi_1 \sinh\phi_2 \ . \tag{3.8}$$

One can solve for ϕ_2 in terms of ϕ_1:

$$e^{2\phi_2} = \frac{\dfrac{\omega_{s1}}{\omega_{s2}} \sin\phi_1 + \cos\phi_1}{\dfrac{\omega_{s1}}{\omega_{s2}} \sin\phi_1 - \cos\phi_1} \ , \tag{3.9}$$

or

$$\sinh\phi_2 = \frac{\cos\phi_1}{\sqrt{\dfrac{\omega_{s1}^2}{\omega_{s2}^2} \sin^2\phi_1 - \cos^2\phi}} \quad \text{and} \quad \cosh\phi_2 = \frac{\dfrac{\omega_{s1}}{\omega_{s2}} \sin\phi_1}{\sqrt{\dfrac{\omega_{s1}^2}{\omega_{s2}^2} \sin^2\phi_1 - \cos^2\phi}} \ . \tag{3.10}$$

Eliminating ϕ_2, the rotation angle ϕ_1 can now be solved Eq. (3.7) in the form

$$-\cos 2\phi_1 = \frac{\left(\dfrac{2|\eta|\delta_0}{\omega_{s2} T_b} \right)^2 - \dfrac{1}{2} \left(\dfrac{\omega_{s1}^2}{\omega_{s2}^2} - 1 \right)}{\dfrac{1}{2} \left(\dfrac{\omega_{s1}^2}{\omega_{s2}^2} + 1 \right)} \ . \tag{3.11}$$

There are 4 parameters in this rf maneuvering. They can be chosen as ω_{s1}, ω_{s2}, ϕ_1, and ϕ_2. So far we have obtained only two relations, Eqs. (3.9) and (3.11), leaving two more variables unrestricted. (Actually ω_{s1} has a minimum; see below for details.) The simulation shown in Fig. 3 is an example with initial half-energy spread $\Delta E = 10$ MeV and $V_1 = V_2 = 4.0$ kV. Comparing with pure rotation, the rf maneuvering time has been reduced from 0.1239 s to 0.1073 s. However, the final beam distribution in the longitudinal phase space is no longer right-rectangular. The parallelogram shape implies larger final momentum spread after 53-MHz recapture. The amount of phase-space dilution can be controlled by suitably choosing ω_{s1} and ω_{s2}.

Let us compute the momentum offsets at the end of the rf maneuvering. Point C' is given by

$$-\frac{|\eta|\delta_2}{\omega_{s2}}\bigg|_{C'} = \tau_1 \sinh\phi_2 - \frac{|\eta|\delta_0}{\omega_{s1}}\cosh\phi_2$$
$$= T_b\Big(\cdots\Big) - \frac{|\eta|\delta_0}{\omega_{s1}}\left(\sin\phi_1\sinh\phi_2 + \frac{\omega_{s1}}{\omega_{s2}}\cos\phi_1\cosh\phi_2\right) , \tag{3.12}$$

while Point B' is given by

$$-\frac{|\eta|\delta_2}{\omega_{s2}}\bigg|_{B'} = T_b\Big(\cdots\Big) + \frac{|\eta|\delta_0}{\omega_{s1}}\left(\sin\phi_1\sinh\phi_2 + \frac{\omega_{s1}}{\omega_{s2}}\cos\phi_1\cosh\phi_2\right) . \tag{3.13}$$

We would like to keep the difference

$$-\frac{|\eta|\Delta\delta_2}{\omega_{s2}} = -\frac{2|\eta|\delta_0}{\omega_{s1}}\left(\sin\phi_1\sinh\phi_2 + \frac{\omega_{s1}}{\omega_{s2}}\cos\phi_1\cosh\phi_2\right) \tag{3.14}$$

to a minimum so as to reduce phase space dilution. Eliminating ϕ_2 with the aid of Eq. (3.9), we arrive at

$$\frac{\Delta\delta_2}{\delta_0} = \left(\frac{\omega_{s2}}{\omega_{s1}} + \frac{\omega_{s1}}{\omega_{s2}}\right)\frac{\sin 2\phi_1}{\sqrt{\dfrac{\omega_{s1}^2}{\omega_{s2}^2}\sin^2\phi_1 - \cos^2\phi_1}} . \tag{3.15}$$

The derivative with respect to ϕ_1 gives

$$\frac{d}{d\phi_1}\frac{\Delta\delta_2}{\delta_0} = -2\left(\frac{\omega_{s2}}{\omega_{s1}} + \frac{\omega_{s1}}{\omega_{s2}}\right)\frac{\cos^4\phi_1 + \dfrac{\omega_{s1}^2}{\omega_{s2}^2}\sin^4\phi_1}{\left(\dfrac{\omega_{s1}^2}{\omega_{s2}^2}\sin^2\phi_1 - \cos^2\phi_1\right)^{3/2}} , \tag{3.16}$$

which is negative definite. This implies that the energy spread difference between Points C' and B' will be reduced when the rotation angle ϕ_1 increases, independent of the choice of ω_{s1} and ω_{s2}. This difference vanishes when $\phi_1 = \pi/2$ according to Eq. (3.15), which is exactly the pure rotation discussed in the previous section. Our conclusion is that the rf maneuvering time can be reduced by the method of a rotation followed by a shear at the expense of some phase-space dilution that cannot be avoided. This conclusion can also be obtained by observing Eq. (3.11) closely. The right-side must lie between ± 1, which is equivalent to saying

$$0 \le \frac{2|\eta|\delta_0}{\omega_{s1}T_b} \le 1 . \tag{3.17}$$

Thus ω_{s1} cannot go below

$$\omega_{s1}\big|_{\min} = \frac{2|\eta|\delta_0}{T_b} , \tag{3.18}$$

which, when compared with Eq. (2.6), is just the angular synchrotron frequency required if a pure rotation for the compression is employed. (For the initial half-energy spread $\Delta E = 10$ MeV, the minimum rotation voltage is $V_1 = 2.823$ kV and the minimum angular synchrotron frequency is $\omega_{s1} = 12.68$ Hz.) We know that pure rotation is the only rf maneuvering that results in a right-rectangular distribution, any larger ω_{s1} employed in a rotation-shear maneuvering will lead to a parallelogram-shape distribution and therefore eventual dilution of phase space.

Let us consider the special case of having $V_1 = V_2$. Then there will be only one free parameter for the rf maneuvering, namely V_1 or ω_{s1}. The solution for ϕ_1 and ϕ_2 reduces to

$$-\cos 2\phi_1 = \left(\frac{2|\eta|\delta_0}{\omega_{s1}T_b}\right)^2 , \tag{3.19}$$

$$\phi_2 = \frac{1}{2}\ln\frac{\tan\phi_1 + 1}{\tan\phi_1 - 1} = \ln\left[\frac{\omega_{s1}T_b}{2|\eta|\delta_0}\sqrt{1+\sin 2\phi_1}\right] . \tag{3.20}$$

At the same time, the fractional increase in longitudinal emittance is

$$\frac{\Delta\delta_2}{4\delta_0} = \frac{\omega_s T_b}{4|\eta|\delta_0}\sin 2\phi_1 . \tag{3.21}$$

The top plot of Fig. 4 shows the total maneuvering time as function of cavity peak voltage when the initial half-energy spread is 4, 6, 8, and 10 MeV. The lower plot shows the fractional increase in eventual phase-space dilution. We see that, comparing with pure rotation, the rotation-shear method does reduce the time of compression, especially when the initial half-energy spread is small. However, as the time of compression is reduced the eventual dilution of phase space increases very fast. We conclude that this method is suitable mostly when the initial half-energy spread is large, like $\Delta E \gtrsim 8$ MeV.

4 ANOTHER ROTATION-SHEAR METHOD

We can have a better understanding of the rf maneuvering in the previous section by concentrating on the axis of the beam PQ originally situated along the arrival-time axis between $\pm T_b$. As indicated in the top plot of Fig. 5, PQ is first rotated along elliptical trajectories to $P'Q'$ and then sheared along hyperbolic trajectories to $P''Q''$. Notice that the rotation of the beam axis from PQ to $P'Q'$ gets past the separatrices provided by V_2 (more than 45° if $V_1 = V_2$). In short, the beam axis has been rotated/sheared by a total of 90° in the whole rf maneuvering. On the other hand, we can also first rotate the beam

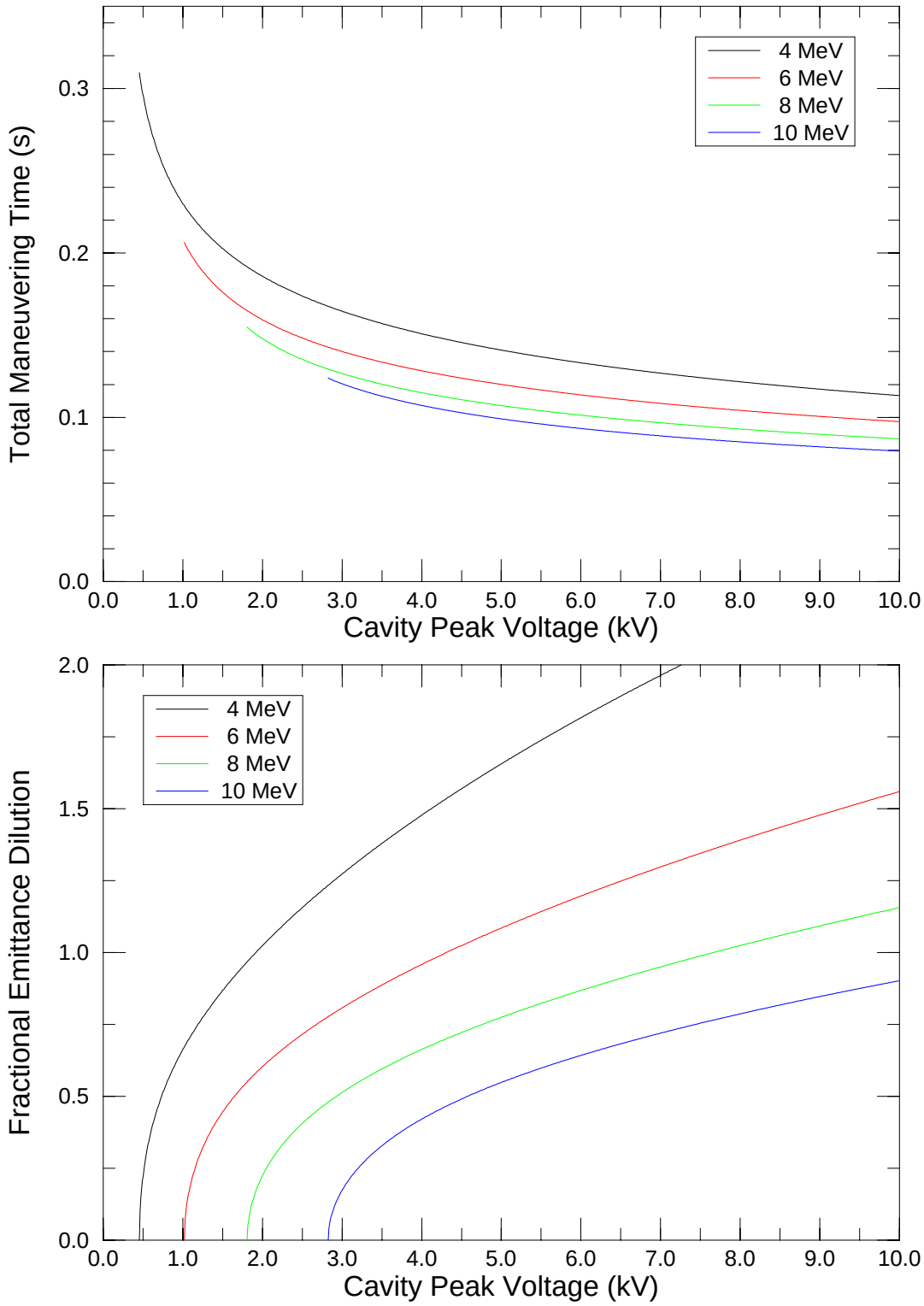

Figure 4: (color) Rotation-shearing maneuvering with equal rotation and shearing voltages, $V_1 = V_2$, showing total maneuvering time (top) and fractional dilution of phase space (bottom) versus cavity peak voltage V_1 for initial half-energy spread $\Delta E = 4$, 6, 8, and 10 MeV.

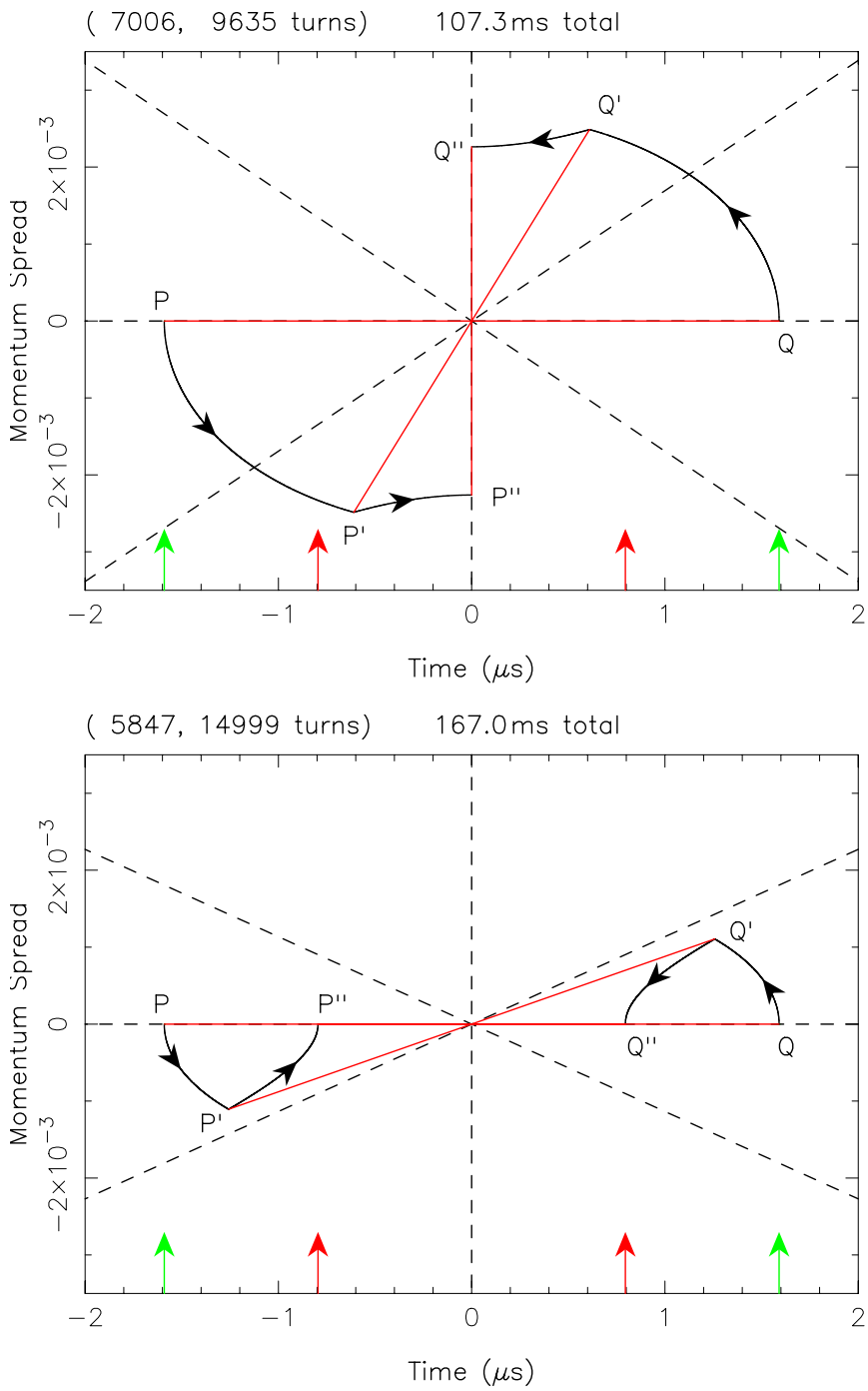

Figure 5: (color) Motion of the beam axis PQ (red) in the longitudinal phase space. It is first rotated to $P'Q'$ along elliptical trajectories and then sheared to $P''Q''$ along hyperbolic trajectories. Top: the rotation gets past the separatrices (dashes) established by V_2 and the total rotation of the beam axis is 90°. Bottom: the rotation does not reach the separatrices and the shear by V_2 moves the beam axis back to the original arrival-time axis.

axis to less than the separatrices set up by V_2 ($< 45°$ if $V_1 = V_2$), and let it shear back to the arrival-time axis landing at $P''Q''$ as illustrated by the lower plot of Fig. 5. The merit of this variation process is that lesser movement of the beam will be required, which may lead to shorter total maneuvering time if the cavity voltages are kept the same as before. In addition, particles having the same energy will remain having the same energy. This is because the rectangular beam will finally be distorted into a parallelogram with the top and bottom sides parallel to the arrival-time axis, as is shown in Fig. 6. If this parallelogram

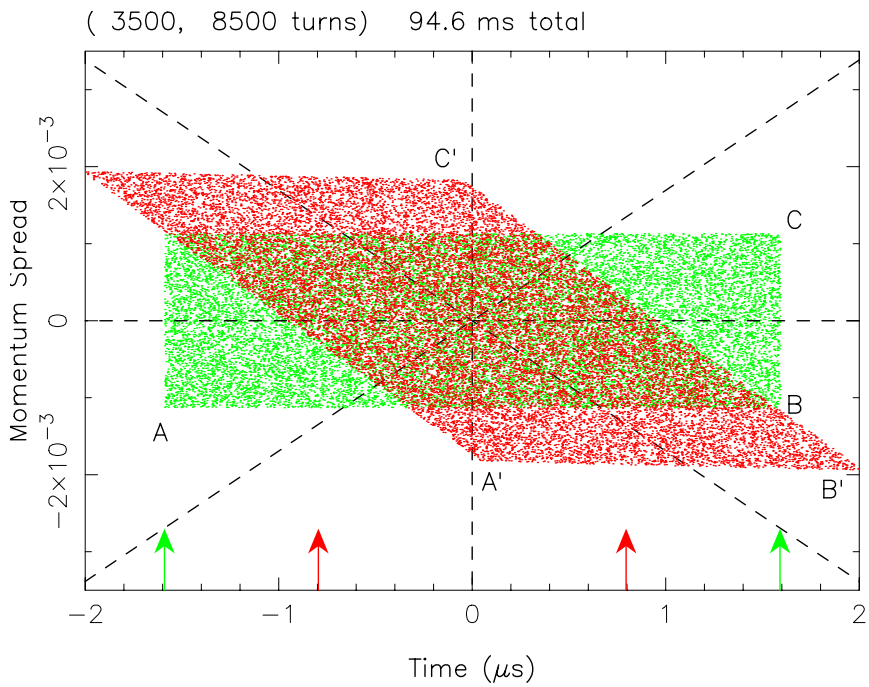

Figure 6: (color) A simulation with the first rotation of the beam axis not reaching the separatrices set up by V_2. The initial beam within $\pm T_b$ is in green. The final beam is in red, distorted into a parallelogram with top and bottom sides parallel to the arrival-time axis. It appears that to contain the final beam within $\pm T_b/2$ is nearly impossible. Note that the corner B' extends farther than the original B. ($V_1 = V_2 = 4.0$ kV have been used with rotation/shear time 3500/4000 turns.)

can be made into an upright rectangle by adjusting other parameters, the compression will have been perfect. Unfortunately, it is extremely difficult, if not impossible, to contain the eventual parallelogram within the desired compressed length $\pm T_b/2$. As is shown in Fig. 6, the corner B', which we want to be at $\tau = T_b/2$, extends farther than the original beam corner B at $\tau = T_b$.

To remedy the situation, Foster et al. [1] propose a way to smooth out these annoying

corners by placing barrier pulses of opposite polarity at both ends of the beam and allow the barrier pulses to move inwards as the beam is compressed. An example is illustrated in Fig. 7. The barrier pulses of opposite voltage polarity are located with their inside edges at the head P and tail Q of the beam axis. As the beam is rotated by the voltage gradient, the barriers are moved inwards so that their inner edges always follow P and Q (lower plot).

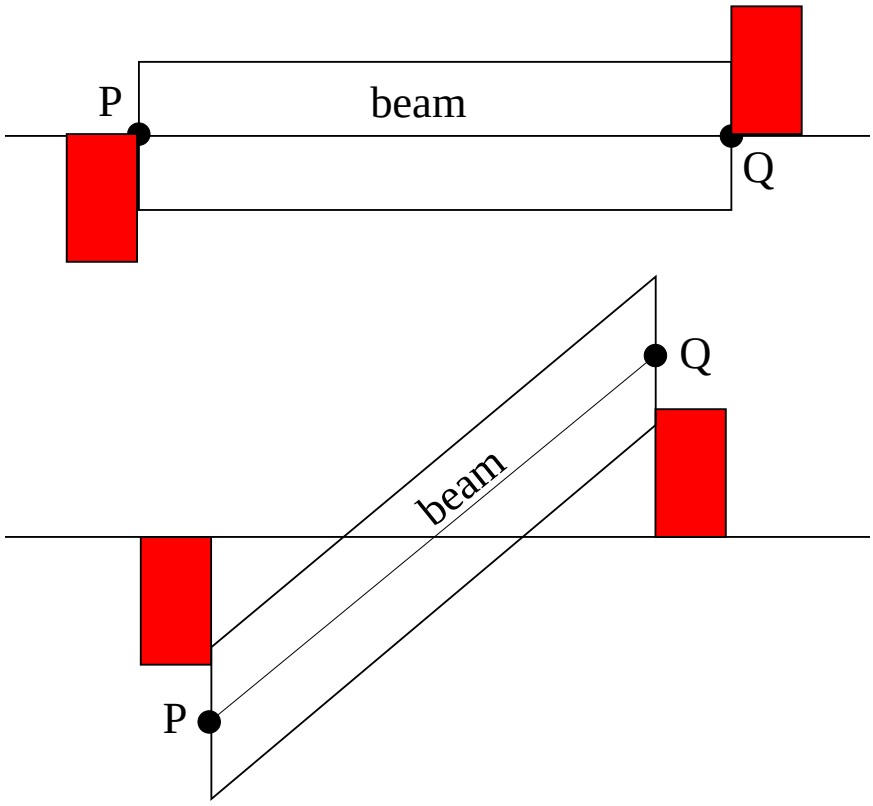

Figure 7: (color) Top: Two barrier pulses (red) of positive and negative voltages are shown flanking the longitudinal length of the beam at P and Q. Bottom: As the beam rotates or shears under a voltage gradient, the barrier pulses move inwards with their inner edges following P and Q.

4.1 Constant Gradient

One version of this method is called *constant voltage gradient*, meaning that all particles will be seeing the same focusing voltage gradient V_1/T_b which remains unchanged during the rotation process. At the same time, all particles will be seeing the same defocusing voltage gradient $-V_2/T_b$ during the compression process.

In order to obtain simple analytic results, we simplify the problem by assuming that the barriers have infinite positive and negative voltages so that there is no penetration into the barriers at all by the beam particles. Let us follow Point Q (in the lower plot of Fig. 5), which starts at $(T_b, 0)$ rotates under voltage gradient V_1/T_b for the angle ϕ_1 to (τ_1, δ_1) and then shears under the voltage gradient $-V_2/T_b$ for the angle ϕ_2 towards $(T_b/2, 0)$. We have

$$\frac{T_b}{2} = \tau_1 \cosh\phi_2 - \frac{|\eta|\delta_1}{\omega_{s2}} \sinh\phi_2 \ , \tag{4.1}$$

$$0 = \tau_1 \sinh\phi_2 - \frac{|\eta|\delta_1}{\omega_{s2}} \cosh\phi_2 \ , \tag{4.2}$$

with

$$\begin{aligned} \tau_1 &= T_b \cos\phi_1 \ , \\ -\frac{|\eta|\delta_1}{\omega_{s1}} &= -T_b \sin\phi_1 \ . \end{aligned} \tag{4.3}$$

From Eq. (4.2), one gets readily

$$e^{2\phi_2} = \frac{\cos\phi_1 + \dfrac{\omega_{s1}}{\omega_{s2}} \sin\phi_1}{\cos\phi_1 - \dfrac{\omega_{s1}}{\omega_{s2}} \sin\phi_1} \ , \tag{4.4}$$

or

$$\cosh\phi_2 = \frac{\cos\phi_1}{\sqrt{\cos^2\phi_1 - \dfrac{\omega_{s1}^2}{\omega_{s2}^2}\sin^2\phi_1}} \qquad \text{and} \qquad \cosh\phi_2 = \frac{\sin\phi_1}{\sqrt{\cos^2\phi_1 - \dfrac{\omega_{s1}^2}{\omega_{s2}^2}\sin^2\phi_1}} \ . \tag{4.5}$$

Eliminating ϕ_2 from Eq. (4.1), we obtain

$$\sqrt{\cos^2\phi_1 - \frac{\omega_{s1}^2}{\omega_{s2}^2}\sin^2\phi_1} = \frac{1}{2} \tag{4.6}$$

or

$$\sin\phi_1 = \frac{\sqrt{3}/2}{\sqrt{1 + \dfrac{\omega_{s1}^2}{\omega_{s2}^2}}} \ . \tag{4.7}$$

To achieve the beam compression, we also need to know the position of the barrier pulses which are moving inwards with Points P and Q, at any moment. The position of Point Q can be evaluated from Eqs. (4.1) and (4.3) and is given by

$$\frac{\tau(t)}{T_b} = \begin{cases} \cos\omega_{s1} t & 0 \le t \le t_1 \ , \\ \cos\phi_1 \cosh\omega_{s2}(t - t_1) + \sin\phi_1 \sinh\omega_{s2}(t - t_1) & t_1 \le t \le t_2 \ , \end{cases} \tag{4.8}$$

where t_1 is the moment when the voltage gradient is flipped and t_2 is the end of the compression.

The problem is now solved. It is interesting to note that the general solution, represented by Eqs. (4.4) and (4.7), depends only on the ratio ω_{s1}/ω_{s2} and it therefore depends on the individual rotation and shearing voltages only when the rotation time and shearing time are evaluated. This indicates that arbitrarily small rotation and shearing voltages will be allowed. The price to pay is, of course, longer maneuvering times. Notice also that the booster batch length T_b does not enter into the solution, implying that the same rotation and shearing angles, ϕ_1 and ϕ_2 will be employed to compress a beam of whatever length to one-half, once the ratio ω_{s1}/ω_{s2} is fixed. Best of all, the initial momentum spread does not enter into the solution. Thus once the rotation and shearing gradients are set, the rotation and shearing times will be fixed independent of the longitudinal emittance of the batches injected from the booster. Since the axis of the beam PQ lands at the time-arrival axis finally, there should be no emittance blowup. The solution depends on $\omega_{s1,s2}$ separately only when time durations are evaluated.

In the special case of $V_1 = V_2$, the solution reads

$$\begin{cases} \phi_1 = \sin^{-1}\dfrac{\sqrt{3}}{2\sqrt{2}} = 0.6591 \ , \\ \phi_2 = \dfrac{1}{2}\ln\dfrac{\sqrt{5}+\sqrt{3}}{\sqrt{5}-\sqrt{3}} = 1.0317 \ . \end{cases} \tag{4.9}$$

The time durations required for focusing and defocusing are, respectively, $\Delta t_1 = \phi_1/\omega_{s1}$ and $\Delta t_2 = \phi_2/\omega_{s2}$.

4.2 Constant Voltage

The focusing and defocusing voltage gradients are generated by broadband cavities by programming the Fourier components of the required waveform. Thus, we can also program the waveform in such a way that the peak voltage attainable by the cavities moves with the head and tail of the beam axis PQ. In this way, Point Q will always be seeing the same accelerating voltage V_1 during the first part of the compression process and same decelerating voltage $-V_2$ during the second part. Hence, we call this method *constant voltage*. Unlike the method of *constant gradient*, here the focusing and defocusing gradients increase gradually

as the compression progresses. We expect, therefore, a relatively shorter compression time than the constant-gradient method.

Because the voltage gradient is changing during the compression process, the Hamiltonian describing the motion of a beam particle is an explicit function of time and the general solution becomes messy. Luckily, a solution of a general beam particle is not necessary. What we actually need is to concentrate on the particle at the tail of the beam axis, or Point Q in the lower plot of Fig. 5. Its motion is governed by the differential equations:

$$\frac{d\tau}{dt} = \eta\delta \ , \tag{4.10}$$

$$\frac{d\delta}{dt} = \frac{eV}{\beta^2 E_0 T_0} \ , \tag{4.11}$$

where $V = V_1$ and $-V_2$, respectively, for the focusing and defocusing portions of the process. Although the angular synchrotron frequencies will no longer be constant, we can still use, as reference, the same angular synchrotron frequencies $\omega_{s1,s2}$ as defined in Eqs. (2.4) and (3.2) at a point T_b away from the center of the longitudinal phase space. The Hamiltonian governing the motion of Point Q is therefore

$$H = -\frac{|\eta|}{2}\,\delta^2 \mp \frac{\omega_{s1,s2}^2 T_b}{|\eta|}\,\tau \ , \tag{4.12}$$

where the minus sign and the subscript $s1$ are for the focusing portion while the positive sign and the subscript $s2$ are for the defocusing portion. Particle Q starts at the initial position (τ_0, δ_0) at time $t_0 = 0$, arrives at position (τ_1, δ_1) at time $t_1 = t_0 + \Delta t_1$ when the voltage gradient flips sign, and finally reaches the position (τ_2, δ_2) at time $t_2 = t_1 + \Delta t_2$. Let us first study the focusing period. The Hamiltonian can be evaluated at the initial condition with $\delta_0 = 0$. Then the momentum spread $\delta(t)$ at any time can be solved. Instead, we can also make use of the equations of motion [Eq. (4.10) and (4.11)] to eliminate dt to get

$$\frac{d\tau}{d\delta} = -\frac{|\eta|^2\delta}{\omega_{s1}^2 T_b} \ . \tag{4.13}$$

An integration gives the trajectory

$$\tau(t) - \tau_0 = -\frac{|\eta|^2}{2\omega_{s1}^2 T_b}\delta^2(t) \ , \tag{4.14}$$

since $\delta_0 = 0$. For $t_1 < t < t_2$, the trajectory is

$$\frac{d\tau}{d\delta} = \frac{|\eta|^2\delta}{\omega_{s2}^2 T_b} \ . \tag{4.15}$$

An integration gives

$$\tau_2 - \tau(t) = -\frac{|\eta|^2}{2\omega_{s2}^2 T_b}\delta^2(t) \ , \tag{4.16}$$

since $\delta_2 = 0$. If the compression ratio is r_{cp}, we can write $\tau_2 = r_{cp}\tau_0$, where τ_0 is the arrival time of Particle Q at start. Then the position of the Point Q at 1 can be readily solved by substituting $t = t_1$ in Eqs. (4.14) and (4.16),

$$\frac{\tau_1}{\tau_0} = \frac{r_{cp}\dfrac{\omega_{s2}^2}{\omega_{s1}^2} + 1}{\dfrac{\omega_{s2}^2}{\omega_{s1}^2} + 1} \ , \qquad \delta_1^2 = \frac{2\omega_{s2}^2 T_b \tau_0}{|\eta|^2}\frac{1 - r_{cp}}{\dfrac{\omega_{s2}^2}{\omega_{s1}^2} + 1} \ . \tag{4.17}$$

Notice that the trajectory of Point Q is no longer elliptic or hyperbolic. It becomes parabolic when the voltage gradient is either focusing or defocusing. The motion is the same as inside a squared barrier pulse, because the voltage experienced by the particle is always the same. On the other hand, the trajectory of a general particle in the beam is much more complicated.

To compute the time duration for the first part of the compression, we first eliminate $\delta(t)$ from Eqs. (4.11) and (4.14) to obtain

$$\frac{d\tau}{\sqrt{\tau_0 - \tau}} = -\sqrt{2\omega_{s1}^2 T_b}\, dt \ . \tag{4.18}$$

An integration from t_0 to t_1 gives

$$\Delta t_1 = \sqrt{\frac{2(\tau_0 - \tau_1)}{\omega_{s1}^2 T_b}} \ . \tag{4.19}$$

Now substitution of τ_1 from Eq. (4.17) leads to

$$\Delta t_1 = \frac{1}{\omega_{s1}}\sqrt{\frac{\tau_0}{T_b}\frac{2(1 - r_{cp})}{1 + \dfrac{\omega_{s1}^2}{\omega_{s2}^2}}} \ . \tag{4.20}$$

The time duration for the second part can be obtained in a similar way. In fact, it is clear that the result will be the same as Eq. (4.20) through the replacement $\omega_{s1} \leftrightarrow \omega_{s2}$, or

$$\Delta t_2 = \frac{1}{\omega_{s2}}\sqrt{\frac{\tau_0}{T_b}\frac{2(1 - r_{cp})}{1 + \dfrac{\omega_{s2}^2}{\omega_{s1}^2}}} \ . \tag{4.21}$$

The total time required is

$$\Delta t_{\text{total}} = \Delta t_1 + \Delta t_2 = \sqrt{\frac{2(1-r)\tau_0}{T_b}\,\frac{1}{\omega_{s1}^2+\omega_{s2}^2}}\ . \tag{4.22}$$

The location of Particle Q, or the location of the inner edge of the right barrier, at time t can be obtained easily by integrating Eq. (4.18) up to t. It is given by

$$\frac{\tau_{_Q}(t)}{\tau_0} = \begin{cases} 1 - \dfrac{T_b}{2\tau_0}\,(\omega_{s1}t)^2 & 0 \le t \le t_1\ , \\[2ex] r_{cp} + \dfrac{T_b}{2\tau_0}\,[\omega_{s2}(t-t_1)]^2 & t_1 \le t \le t_2\ , \end{cases} \tag{4.23}$$

In the special case of $V_1 = V_2$, $\tau_0 = T_b$, and a compression ratio $r_{cp} = \frac{1}{2}$, the rotation and shear durations reduce to

$$\Delta t_1 = \Delta t_2 = \frac{1}{\sqrt{2}\,\omega_{s1}} \qquad \text{and} \qquad \Delta t_{\text{total}} = \frac{\sqrt{2}}{\omega_{s1}}\ . \tag{4.24}$$

In comparison with the method of constant gradient, where the total compression time stated in Eq. (4.9) is

$$\Delta t_{\text{total}} = \frac{1}{\omega_{s1}}\left(\sin^{-1}\frac{\sqrt{3}}{2\sqrt{2}} + \frac{1}{2}\ln\frac{\sqrt{5}+\sqrt{3}}{\sqrt{5}-\sqrt{3}}\right) = \frac{1.6908}{\omega_{s1}}\ , \tag{4.25}$$

the reduction has been 16.4%.

If we have interest in the behavior of the beam at any time, we must address the motion of a general particle. The phase equation is the same as Eq. (4.10). But the momentum equation becomes

$$\frac{d\delta}{dt} = \pm\frac{eV_{1,2}}{\beta^2 E_0 T_0}\frac{\tau}{\tau_{_Q}(t)} = \pm\frac{\omega_{s1,s2}^2 T_b}{|\eta|}\frac{\tau}{\tau_{_Q}(t)}\ . \tag{4.26}$$

The appearance of $\tau_{_Q}(t)$ in the momentum equation is due to the fact that the arrival time of Particle Q determines the position at which the voltage is set at V_1 (or $-V_2$). In any case, the Hamiltonian becomes explicitly time dependent making analytic solution much more difficult. Obviously, the voltage a general particle experienced will not be constant in time, and its trajectory will not be parabolic. Fortunately, such solution will not be necessary at all in understanding the compression process. Equation (4.26) is needed only for tracking, where we do not even require the expression of $\tau_{_Q}(t)$ stated by Eq. (4.23), because $\tau_{_Q}$ will be provided by tracking also.

4.3 Application to the Main Injector

In the Main Injector, the voltage gradient can be generated using the 3 longitudinal dampers each providing 600 V (or $V_1 = V_2 = 1.8$ kV). The reference angular synchrotron frequencies for rotation and shearing with voltages V_1 and $-V_2$ at distance T_b from the beam center are $\omega_{s1} = \omega s2 = 10.125$ Hz. The rotation time and shearing times are both 69.8 ms (6273 turns) in the constant-voltage method. The total process takes 140 ms or 2.1 booster cycles. A simulation of compressing a two-booster-batch beam with initial half-energy spread 10 MeV is illustrated in Fig. 8. The tracking results using the method of *constant gradient* are similar. But the time durations for rotation and shear are, respectively, 65.1 ms (5847 turns) and 102 ms (9151 turns). The total time of compression is increased to 167 ms or 14998 turns.

In Fig. 8, the barrier pulse voltages used in the simulation have been as high as 100 kV. In reality, barrier pulses will be generated from a Finemet cavity in the Main Injector and the maximum barrier voltage attainable is only ± 6.25 kV. Unfortunately this Finemet cavity is not capable of generating desirable waveforms because it is not broadband programmable; it works like a transformer where the primary current is regulated by a high-voltage fast switch. [7] Otherwise, we can use it to boost the rotation/shear gradients and the compression time will be greatly reduced. As a generator of squared barrier pulses, the ± 6.25 kV is still not large enough. However, we can always make use of the dampers to generate a constant 1.8 kV inside the squared barrier, thus boosting the barrier voltage to $V_b = \pm 8.05$ kV.

For a simulation with a finite barrier voltage, we first populate beam particles into the barrier buckets with total width $2T_b$ including the penetration. The penetration τ_p (in time) can be computed easily from the Hamiltonian

$$H = -\frac{|\eta|\delta^2}{2} - \frac{eV_b}{\beta^2 E_0 T_0}\,\tau_p \ . \tag{4.27}$$

The maximum penetration for a momentum spread of the beam δ_0 is

$$\tau_{p0} = \frac{|\eta|\beta^2 E_0 T_0}{2eV_b}\delta_0^2 \ , \tag{4.28}$$

which is 0.08983 μs/0.02246 μs when the initial half-energy spread is 10 MeV/5 MeV. If we wish to compress the beam of half length T_b to one of half length $T_b/2$ including penetration, the actual compression of the beam outside the barriers will be from half length $\tau_0 = T_b - \tau_{p0}$ to half length $\tau_2 = T_b/2 - 4\tau_{p0}$, or a compression ratio of

$$r_{\rm cp} = \frac{T_b/2 - 4\tau_{p0}}{T_b - \tau_{p0}} \ , \tag{4.29}$$

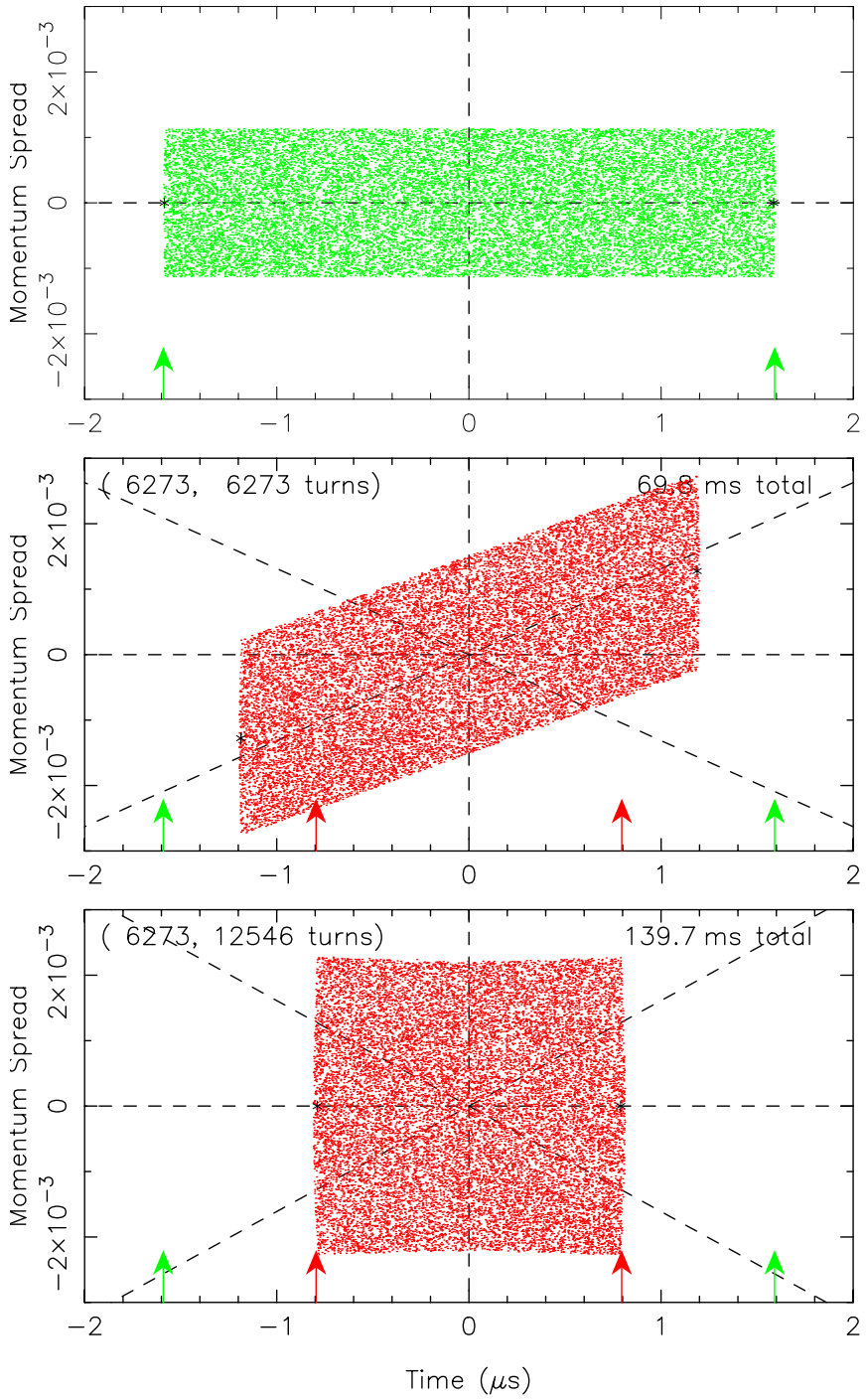

Figure 8: (color) A beam of original total length $2T_b$ and half-energy spread 10 MeV (top) is compressed using the method of constant voltage first at 1.8 kV for 6273 turns (middle), then at -1.8 kV for 6273 turns (bottom). The total length of the beam is compressed to T_b. At all times, the beam is flanked by two barrier pulses of opposite polarity with their inner edges touching the head and tail of the beam axis. Barrier voltages much larger than ± 100 kV have been used as an illustration. The instantaneous separatrices set up by $-V_2$ are also shown.

which is less than $\frac{1}{2}$. Thus, we expect the rotation and shear time durations will become longer.[§]

Simulations with barrier voltage at ± 8.05 kV have been performed. The results are shown in the top-left plot of Fig. 9 for initial half-energy spread 10 MeV and in the bottom-left plot for initial half-energy spread 5 MeV. The rotation and shear voltages are set at ± 1.8 kV at the inner edge of the barriers. Comparing with the bottom plot of Fig. 8, the total compression time is 161 ms for the 10 MeV half-energy-spread beam and 145 ms for the 5 MeV half-energy-spread beam. The final momentum spread becomes slightly larger than double the initial values.

4.4 Function of the Barriers

It is worth pointing out that the barrier pulses, although moving inwards, are only doing the job of limiting the expansion of the corners of the beam distribution by reflecting them and the actual compression is done by the focusing voltage gradient and defocusing voltage gradient. Without the voltage gradients, the inwards-moving barriers will lead to gaps in the beam distribution and eventual dilution of phase space. The latter can only be avoided if the barrier moving rate $\dot{T}$ satisfies the adiabatic condition [10]

$$|\dot{T}| \ll \frac{1}{2}|\eta|\delta \ , \tag{4.30}$$

where δ is the half-momentum spread of the beam. According to the top-left plot of Fig. 9, the barriers are moving at the average rate of $\dot{T} = T_b(1 - r_{\rm cp})/T_{\rm cp} = 7.52 \times 10^{-6}$, where $T_{\rm cp} = 0.140$ s is the total time of the compression process when the initial half-energy spread is 10 MeV. To satisfy adiabaticity, the half-momentum spread must be $\delta \gg 1.87 \times 10^{-3}$ or the half-energy spread must be $\Delta E \gg 14.9$ MeV. Thus adiabaticity cannot be satisfied even when the half-energy spread of the beam is 10 MeV, and will be much worse when the half-energy spread is 5 MeV. Simulations with only moving barriers but no focusing and defocusing voltage gradients are shown in the top-right plot of Fig. 9 for initial half-energy spread 10 MeV and bottom-right plot for initial half-energy spread 5 MeV. These are to be

[§]In the constant-gradient method, the new rotation phase and shear phase can be obtained easily by modifying the left-side of Eq. (4.1) by $\tau_0 r_{\rm cp}$, the right-side of Eq. (4.6) by $r_{\rm cp}$, and the left-side of Eq. (4.8) by $\tau(t)/\tau_0$. The solution of the rotation phase ϕ_1 in Eq. (4.7) becomes $\sin\phi_1 = \sqrt{(1 - r_{\rm cp}^2)/(1 + \omega_{s1}^2/\omega_{s2}^2)}$. Because of the special nature of constant gradient, the rotation and shear time durations depend on the compression ratio r_{cp} only and is independent of the initial half-length τ_0 of the beam.

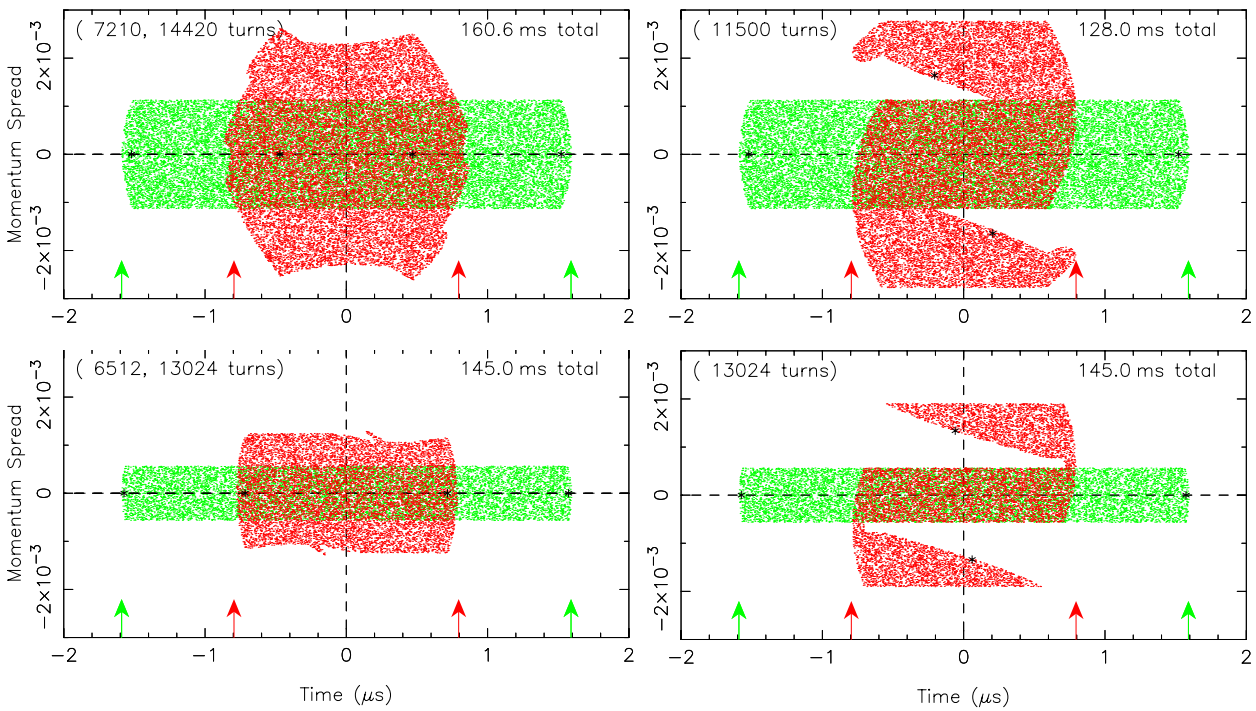

Figure 9: (color) Final distribution of a compressed beam (red) of original total length $2T_b$ with barrier pulses of ± 8.05 kV flanking both ends. The top-left and top-right are for initial half-energy spread 10 MeV while the bottom-left and bottom-right are for initial half-energy spread of 5 MeV. Voltage gradients, with cavity voltages ± 1.8 kV following the head and tail ends of the beam axis, are employed to the top-left and bottom-left, while no voltage gradients are used in the top-right and bottom-right.

compared with the simulations plotted on the left, where focusing and defocusing voltage gradients are present. We do see large empty spaces generated in the beam distribution in the 5 MeV situation. In the 10 MeV situation, the compression time is somewhat shorter than when the voltage gradients are present. This adjustment is required in order to keep the final beam within $\pm T_b/2$ and at the same time not to let the momentum spread become too large.

For a stationary barrier with positive voltage, any particle that enters the barrier from the left with negative momentum offset δ_i (< 0) will leave the barrier in the opposite direction with positive momentum offset $\delta_f = -\delta_i$. For a barrier moving to the left with velocity $\dot{T}$, it will just catch up with particles moving to the left with momentum offset $\delta_{\rm sfp} = \dot{T}/|\eta|$ and they appear to be stationary to the moving barrier. In other words, they form the line of stable fixed points in the frame of the moving barrier. A particle with momentum offset

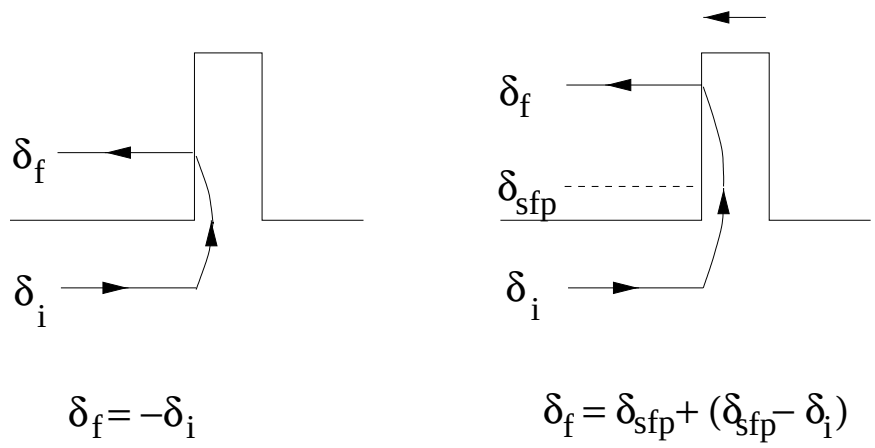

Figure 10: Left: Particles with momentum offset δ_i enters a stationary barrier and comes out with momentum offset $\delta_f = -\delta_i$. Right: The barrier is moving to the right with the same velocity as the particles, having momentum offset $\delta_{\rm sfp}$, shown as dashes. Particles entering the moving barrier will have its momentum reflected about $\delta_{\rm sfp}$, so that the final momentum offset is $\delta_f = \delta_{\rm sfp} + (\delta_{\rm sfp} - \delta_i)$.

$\delta_i < \delta_{\rm sfp}$ encountering the barrier will have its momentum offset reflected about $\delta_{\rm sfp}$ when it departs the barrier; the final reflected momentum offset becomes $\delta_f = \delta_{\rm sfp} + (\delta_{\rm sfp} - \delta_i)$. This is illustrated in Fig. 10.

The right barrier pulse in this rf maneuvering moves at the speed of Point Q, which is the tail of the beam axis (see, for example, Fig. 7), and it therefore sees Point Q as a stable fixed point. Thus, particle encountering the barrier will be reflected about Point Q. If the positive momentum spread and negative momentum spread are equal and opposite, all particles entering the barrier will merge after reflection into the positive energy spread distribution smoothly without making any disturbance into the distribution. Although this is not true during rotation and shear, the positive and negative momentum spreads in general will not differ by too much during the compression process. As a result, the disturbance into the beam distribution will not be big and that explains the absence of empty spaces in the simulations in the top-left and bottom-left of Fig. 9.

Let us follow the compression process more closely. At the beginning of the rotation, we find near Point Q slightly larger positive momentum spread than negative momentum spread. Thus particles are reflected by the right barrier to not as large positive momentum spread as the original beam, exhibiting a deficiency in particles at the top edge of the beam near Q. However, the reverse happens when the beam approaches the end of the rotation before the

gradient flip. Thus, particles are reflected to larger positive momentum spread, resulting in excess particles at the top edge of the beam near Q. After reversing the voltage gradient and until the end of the shear process, the positive and negative momentum spreads gradually become equal and opposite again. This explains why ripples and wavy edges are seen in the beam distributions in the top-left and bottom-left plots in Fig. 9. But there should not be as much empty spaces in the distribution when only barriers are present without the voltage gradients.

Before the flip of the voltage gradient, compared with Point Q, particles entering the right barrier starts to see an extra voltage of 6.25 kV, (seeing 1.8 kV before entering and 6.25 + 1.8 kV after entering). Just after the flip of the voltage gradient, particles will see instead the extra voltage of 9.85 kV, (seeing -1.8 kV at Point Q before entering but 6.25+1.8 kV once inside the barrier). When they emerge from the barrier, these particles will acquire exactly the same positive momentum spreads equal and opposite to their negative momentum spreads at entrance. Only those particles that are already inside the barrier when the voltage flip takes place will have their emergent momentum spreads affected. Consider, for example, a particle that is already at its deepest barrier penetration when the voltage gradient is flipped. This particle reaches this penetration by losing 6.25 kV per turn from the moment its enters the barrier. Now it is gaining 9.85 kV per turn on its way out and will therefore exit with positive momentum spread larger than the negative of its incident momentum spread. From Eq. (4.28), the ratio of exit to incident momentum spreads is

$$\frac{\delta_{\text{exit}}}{\delta_{\text{incident}}} = \sqrt{\frac{V_{\text{after}}}{V_{\text{before}}}} \ , \tag{4.31}$$

where $V_{\text{after}} = 9.85$ kV is the relative barrier voltage after the gradient flip and $V_{\text{before}} = 6.00$ kV is the relative barrier voltage before the flip. The result is a sudden momentum spread enhancement of 28%, which explains the two finger-like bumps, one pointing to the top-left and the other pointing to the bottom-right, [11] in the bottom-left plot of Fig. 9, where the initial half-energy spread is 5 MeV. The same enhancement occurs when the initial half-energy spread is 10 MeV in the top-left plot. The two bumps are not so pronounced, because, first, they are much broader since it takes more time for particles at a half-energy spread of 10 MeV to clear the barriers than if the half spread is 5 MeV, and, second, it just happens that these bumps move to the top-left and bottom right corners of the distribution at the end of the compression. One way to remove these two bumps is to increase the excess 3.6 kV in the barrier slowly rather than abruptly after the gradient flip.

5 CONCLUSIONS

We have studied the compression of a beam by a factor of two using various rf gymnastics and derived simple analytic formulas for each method. Our conclusions are as follows:

1. The simplest way is just a pure rotation. However, the rotation voltage gradient is determined exactly by the initial momentum spread of the beam. The smaller the momentum spread, the smaller the rotation gradient and the longer the compression time. No confining barriers are required.

2. Next we studied rotation in focusing voltage gradient along elliptic trajectories followed by shear in defocusing voltage gradient along hyperbolic trajectories. One way is to have the beam axis rotated past the separatrices set up by the defocusing voltage gradient ($> 45°$ when the rotation and shear voltage gradients are equal and opposite). This method essentially rotates the beam by 90° in less time depending on the cavity voltage, which must be larger than some minimum value determined by the initial momentum spread of the beam. There will be eventual phase-space dilution after the 53-MHz recapture. The dilution increases as this rotation/shear method deviates more from a pure rotation. No confining barriers are required.

3. A variation of the rotation/shear method is to rotate the beam axis by a smaller amount not to get past the separatrices set up by the defocusing voltage gradient ($< 45°$ when the rotation and shear voltage gradients are equal and opposite), so that the beam axis shears back to its original position but compressed. Unfortunately, some corners of the final parallelogram-shape beam distribution extend past the original beam head and tail, so that the whole beam has not been compressed although the beam axis has. Fortunately, barrier pulses can be placed on both sides to limit the spread of these far-extending corners. This barrier-added rotation-shear method is nice because the amounts of rotation and shear do not depend on the original momentum spread of the beam and the longitudinal emittance is preserved. At the same time, there is no restriction on the sizes of the focusing and defocusing voltage gradients.

4. There are two variations of the barrier-added rotation-shear method. One is constant gradient and the other one is constant voltage. In the constant voltage scheme, the peak rotation/shear voltage sticks to the ends of the original beam axis. This variation is more appealing because the rotation and shear gradients will be effectively larger, thus the total compression time will be reduced.

5. The application of the barrier-added rotation-shear method to the Main Injector has been discussed with the voltage gradients generated by the 3 longitudinal broadband dampers. Special attention has been paid to the penetration of the beam into the squared-wave barrier which can attain a maximum voltage of ± 8.05 kV, when we combine the ± 6.25 kV of the Finemet cavities and the 1.8 kV of the dampers.

6. The function of the barrier pulses in the barrier-added rotation-shear method has been analyzed to demonstrate that it is the voltage gradients and not barriers that are performing the beam compression.

References

[1] The originators of this method for the Fermilab Main Injector include G.W. Foster, C.M. Bhat, J. MacLachlan, and J. Griffin.

[2] Fermilab Accelerator Division, *Run II Handbook*, http://www-bd.fnal.gov/runII.

[3] C. Ankenbrandt, *"SLIP-STACKING": A New Method of Momentum-Stacking*, Fermilab Report FN-352, 1981; F.E. Mills, *Stability of Phase Oscillations under two Applied Frequencies*, BNL Internal Report AADD 176, 1971; D. Boussard and Y. Miszumachi, IEEE Trans. Nucl. Sc. **NS-26**, 3623 (1979); J.P. Delahaye, P. Lefevre, and J.P. Riunaud, IEEE Trans. Nucl. Sc. **NS-26**, 3565 (1979).

[4] K. Seiya, Private communication.

[5] J. Griffin, C. Ankenbrandt, J.A. MacLachlan, A. Moretti, IEEE Trans. Nucl Science, NS**30**, 3502 (1983); V.K. Bharadwaj, J.E. Griffin, D.J. Harding, J.A. MacLachlan, IEEE Trans. Nucl. Science NS**34**, 1025 (1987).

[6] G.W. Foster, D.J. Nichlaus, W. Schappert, and D.W. Wildman, *MI/RR Damper* Fermilab Accelerator Division Document Database Beams-doc-605-v1, 2003

[7] W. Chou, J. Griffin, K.Y. Ng, D. Wildman, A. Takagi, and H. Zheng, *Barrier Rf Stacking at Fermilab*, Proc. 2003 Part. Acc. Conf. May 12-16, Portland, Oregon.

[8] C.M. Bhat, B. Chase, G.W. Foster, J. MacLachlan, K. Seiya, P. Varghese, and D. Wildman, *Fermilab Recycler Machine Log Book*, November 20, 2002 183337log *Fast Stacking*; December 12, 2002 090424log *Fast Stacking*; *Fermilab Main Injector Machine Log Book*, February 23, 2003 193916log *Fast Stacking*.

[9] A. Friedman, et al, PAC'95, *Progress Toward a Prototype Recirculating Induction Accelerator for Heavy-Ion Fusion*, Proc. 1995 Part. Acc. Conf. and Int. Conf. High Energy Acc., May 1-5, 1995, Dallas, Texas, p.828.

[10] K.Y. Ng, *Multiple Injections with Barrier Buckets*, Proc. 1997 Particle Accel. Conference, Vancouver, B.C., Canada, 12-16 May, 1997, p.1003; K.Y. Ng, *Injection of JHP Main Ring Using Barrier Buckets*, Fermilab Internal Report FN-0654, 1997.

[11] G.W. Foster, private communication.